

# Embossable grating couplers for planar evanescent wave sensors

## P. KARASIŃSKI\*

Department of Optoelectronics, Silesian University of Technology, 2 Krzywoustego Str., 44-100 Gliwice, Poland

The paper presents input grating couplers to be applied in planar evanescent wave sensors. Waveguide films  $SiO_2$ : $TiO_2$  were obtained using the sol-gel method, and grating couplers with a groove density of 1000 g/mm and 2400 g/mm were produced using the method of master grating embossing in sol film. The influence of refractive index of the cover on incoupling angles was presented. Basing on the experimental results, detection limits involving the changes of effective indexes and refractive indexes of the cover for the investigated planar structures were determined. Sensor structures with the couplers having a groove density of 1000 g/mm enable to detect minimum changes of the effective index below  $3.3 \times 10^{-7}$  and to detect minimum changes of refractive index of the cover below  $2.3 \times 10^{-6}$ . Detection limits for the structures with couplers having the groove density of 2400 g/mm are over twofold higher.

**Keywords:** grating coupler, evanescent wave sensor, sol-gel.

## 1. Introduction

Optical sensors and biosensors have been increasingly gaining attention in the world of scientific research. The said sensors may find numerous applications in environment monitoring, in food control, in pharmacology and medicine. By the application of optical transducers in chemo- or biosensor systems, we can potentially generate very high sensitivities. It particularly involves planar evanescent wave sensors. Due to the applied manufacturing technology, planar sensor structures are relatively easy to optimise. The main physical effects used in planar evanescent wave chemical and biochemical sensors are as follows: the change of refractive index of waveguide cover in the sensor structure and the change of sensitive film thickness [1–3]. The said effects bring about the change of effective refractive indexes of modes propagating in the structure. The changes of effective refractive indexes can be measured by the application of the interferometers of Mach-Zehnder [4,5], Young [6,7] and with a polarimeter [1,8–10] or grating couplers [3,11–18]. In chemical and biochemical measurements, surface plasmon resonance sensors are also applied [19,20].

Grating couplers allow us to measure effective refractive indexes with high accuracy. Therefore they can be applied to determine the absolute value of the refractive index of the uniform cover or to determine the thickness and the refractive index of the sensitive film. Grating couplers as sensor elements were for the first time applied by the research team led by Lukosz [11,12]. The application of grating couplers for sensor application has been also intensively investigated by Kuntz *et al.* [13–15], and by Vörös, Szendrö, and Horváth

The presented paper involves input grating couplers for the application in planar evanescent wave sensors. Grating couplers with the groove density of 1000 g/mm and 2400 g/mm have been fabricated in sol-gel derived silica-titania waveguide films of high refractive indexes. Waveguide structures were investigated in a goniometric system, in which the influence of refractive index of the cover on incoupling angles was determined. The paper describes the determination procedure of maximum incoupling peak position. For the structure with the groove density of 1000 g/mm, the determination procedure of the normal was presented basing on incoupling peaks corresponding to two different diffraction orders. Basing on the experimental results, angular sensitivities of sensor structures were determined. Taking into consideration the angular detection limit of the goniometric system, the detection limits involving the changes of effective indexes and refractive indexes of the cover were determined. The results obtained for both structures of

<sup>[16,17].</sup> Commercial measurement systems based on input grating couplers are already available [18]. Owing to high measurement sensitivities, which can be obtained with the application of grating couplers and due to a relatively easy measurement method, grating couplers and sensor structures based on them are still being investigated in many scientific research centres. The technologies of planar evanescent wave sensors are most frequently based on waveguide films from metal oxides having high refractive indexes in the visible range of spectrum. Such waveguide films can be produced with the application of commercially available vacuum evaporators and sputtering equipment. However, they are too expensive for medium-volume sensor production. An economical and highly effective method for planar waveguide fabrication is the sol-gel technique [16,21].

<sup>\*</sup>e-mail: pawel.karasinski@polsl.pl

different groove density have been compared, and the influence of grating coupler period on angular sensitivity has been discussed. The experimental results have been compared with the results of theoretical analysis.

# 2. Grating coupler

The grating coupler is a periodic corrugation of the period  $\Lambda$  produced in a planar waveguide. The excitation diagram of a planar waveguide from the substrate's side with the use of a grating coupler is presented in Fig. 1. The figure is out of scale. The coupler is illuminated at the angle  $\theta$  with a monochromatic light beam of the wavelength  $\lambda$ . When the incidence angle performs the condition [1]

$$(\pm)N = n_p \sin \theta_r + r \lambda / \Lambda, \tag{1}$$

then, the excitation of the mode of the effective refractive index N is taking place. The (+) or the (-), respectively, has to be chosen if the mode propagates along the +x or -x direction. In Eq. (1),  $r = \pm 1, \pm 2, \pm 3...$  stands for diffraction order and  $n_p$  is the refractive index of the medium in which the angle  $\theta_r$  is measured. The same relation is accepted when guiding the light out from the waveguide. However, in the experimental part of the work we present only the results for the input coupler. Higher incoupling efficiencies are obtained when the structure is excited from the substrate side, as it was presented in Fig. 1. The dependences of the incoupling angle  $\theta$  on the grating period  $\Lambda$  for the first five diffraction orders are presented in Fig. 2. The presented dependences correspond to the wavelength  $\lambda = 676.7$  nm and to the effective refractive index N = 1.51. It can be observed that in each diffraction order, the incoupling angle can be positive or negative. The diagram of the sensor structure excited with the positive angle  $\theta$  is presented in Fig. 1. The negative angle  $\theta$  means that the light beam is projected from the right-hand side of the normal (Fig. 1), and the excited mode is also propagating to the right. Since the incoupling efficiency is decreasing with the rise of the diffraction order r of the grating and is increasing with the rise of incoupling angle [22], therefore the excitation of structures in the orders higher than r = 2 is not used in practice, and the grating periods  $\Lambda$  do not generally exceed 1 µm. The incoupling efficiency is also dependent on corrugation depth, coupler length and the dimensions of the illuminating light beam [23].

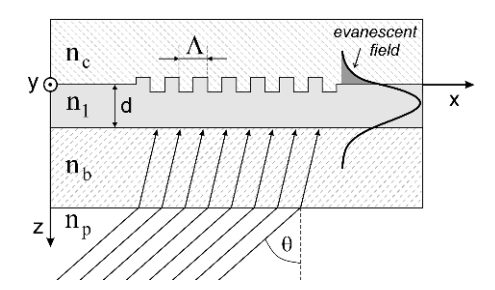


Fig. 1. Diagram involving excitation of planar waveguide with application of a grating coupler.

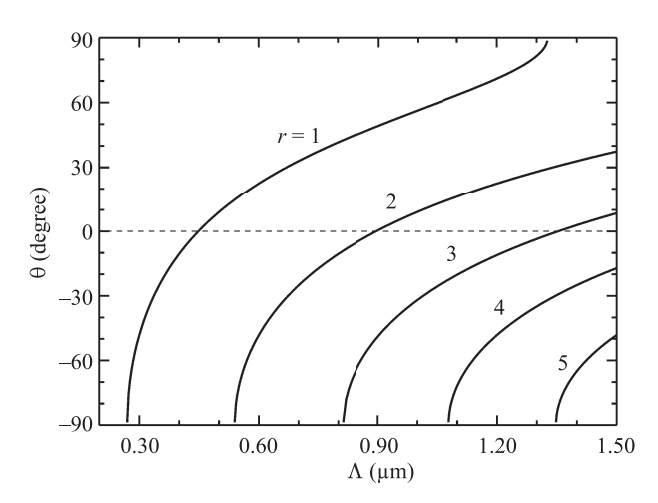


Fig. 2. Incoupling angle vs. grating period for the effective index N = 1.51 and the wavelength  $\lambda = 676.7$  nm.

The changes of refractive index of the cover of the waveguide or the changes of sensitive film thickness result from the changes of effective refractive indexes. In the present paper we will be investigating the changes of refractive index of the cover only, i.e., it has been assumed that the measurand is homogeneously distributed in the cover. When the changes of refractive index of the cover  $\Delta n_c$  are small, then the corresponding to them changes of incoupling angle can be written as

$$\Delta\theta = \left(\frac{\partial\theta}{\partial n_c}\right) \Delta n_c = \left(\frac{\partial\theta}{\partial N}\right) \left(\frac{\partial N}{\partial n_c}\right) \Delta n_c, \qquad (2)$$

where  $\partial\theta/\partial n_c$  is the angular sensitivity of the sensor structure to the changes of the refractive index of the cover,  $\partial\theta/\partial N$  stands for the coupler's sensitivity to the changes of the effective refractive index, and  $\partial N/\partial n_c$  stands for homogeneous sensitivity. This equation is used as a basis for both input and output grating coupler sensors. The changes of refractive index of the cover bring about the changes of the effective refractive index N of the guided mode. These changes are characterized by the homogeneous sensitivity  $\partial N/\partial n_c$ . The following is obtained from the equation (1)

$$\frac{\partial \theta}{\partial N} = \left[ n_p^2 - \left( n - r \frac{\lambda}{\Lambda} \right)^2 \right]^{-1/2}.$$
 (3)

The dependences of the sensitivity  $\partial\theta/\partial N$  on the grating period  $\Lambda$  for the first and second diffraction orders are presented in Fig. 3. Both dependences are non-monotonic and their minimums occur for the grating period  $\Lambda = r\lambda/N$ , whereas the minimum values of the sensitivity  $(\partial\theta/\partial N)_{\min} = n_p^{-1} \operatorname{rad} \approx 180/\pi \operatorname{degree-RIU}^{-1}$  (RIU – refractive index unit).

## 3. Technology

Two-component silica-titania waveguide films SiO<sub>2</sub>:TiO<sub>2</sub> of high refractive index were produced in sol-gel technology with the application of tetraethylorthosilicate

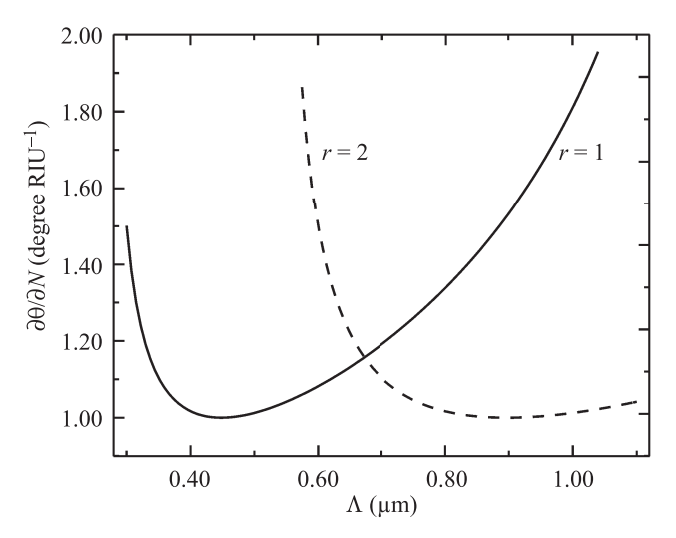


Fig. 3. Grating coupler sensitivity on effective refractive index change vs. grating period for N = 1.51 and  $\lambda = 676.7$  nm.

 $Si(OC_2H_5)_4$  and tetraethyl orthotitanate  $Ti(OC_2H_5)_4$  as the precursors respectively of silica and titania [24,25]. The films on the soda-lime glass substrates  $(n_b = 1.509)$  were deposited using the dip-coating method. The basic parameter used to control the thickness d of the produced films in the dip-coating method is substrate withdrawal speed from sol v. Figure 4 presents the influence of substrate withdrawal speed v on the thickness d and on the refractive index n of films, which, after being coated, were calcined at 773 K (500°C) for 1 h. Open squares and open triangles were used to mark experimental points. The dependence of the thickness d on the substrate withdrawal speed v was approximated with the function  $d = Av^{\alpha} + B$  (solid line) [24], and the dependence of the refractive index n on the speed v was approximated with a linear function (dashed line). Basing on the uncertainty of the approximation parameters d = d(v)and n = n(v) it was determined that the scatter of the refractive indexes of films obtained in the same technological process does not exceed 0.7%, and the scatter of film thickness

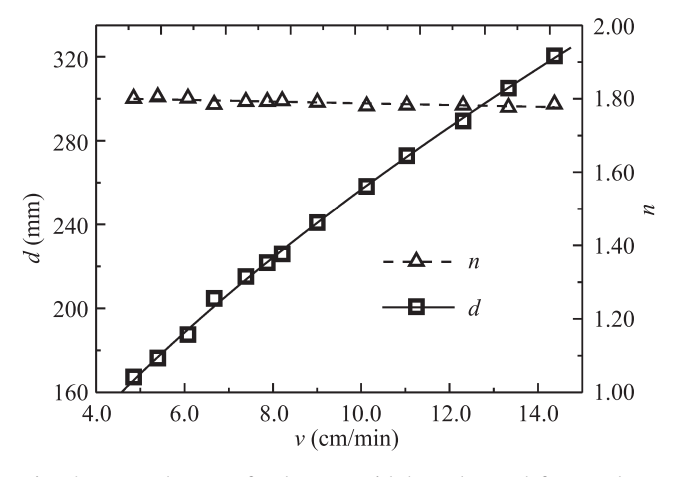


Fig. 4. Dependences of substrate withdrawal speed from sol on waveguide film thickness and refractive index, respectively.

is lower than 2%. And the scatter of the refractive index of the films  $SiO_2$ : $TiO_2$  produced in different technological processes do not exceed 1.5%. The repeatability of the parameters involving the presented here waveguide films obtained using the sol-gel method is comparable to the repeatability obtained with the LPCVD method [26]. The produced waveguide films were single-mode ones and they were characterized by excellent smoothness and low optical loss (below 0.5 dB/cm) [27].

After the sol film had been deposited on the substrate, a relief of the grating coupler was embossed in it. The procedures described in Refs. 22, 28, and 29 were followed. The process yielded couplers with the groove density of  $\chi$ = 1000 g/mm and couplers with the groove density of  $\chi$  = 2400 g/mm. In all cases, the coupler length was  $L_g \sim 2$  mm. The couplers of the groove density  $\chi = 1000$  g/mm were produced with the application of silicon master gratings. The master gratings were produced in silicon substrates with the application of electronolithographic processes and ion etching at ITME (the Institute of Electronic Materials Technology, Warsaw, Poland). After the embossing of master grating in the sol film, the structures were calcined at 673 K (400°C) for 1.5 h. Ultimately, the refractive index of the waveguide films in the produced structures was  $n_1 =$ 1.7609. Figure 5 presents a microscopic image of the coupler obtained with the application of difference interference (microscope BIOLAR PI, Poland). The corrugation amplitude of the waveguide film was  $\sigma = 9$  nm. An important parameter to be followed in the technology involves a long-term stability of the produced structures. The structures whose research results are presented below had been produced 2 years earlier before they were applied in the presented here research studies. The ellipsometric measurements of waveguide films produced at different times over the period of 2 years did not show any changes of thickness or refractive index. Also the measurements of attenuation did not result in the rise of optical loss. An extensive characteristic of the elaborated waveguide films will be presented in Ref. 30.

The couplers of the groove density  $\chi = 2400$  g/mm were produced with the application of commercially available

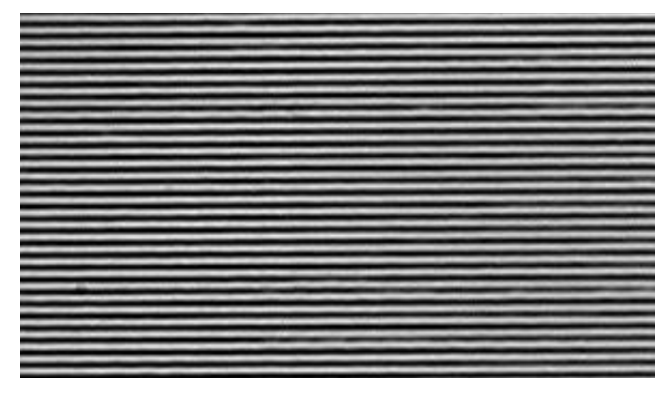


Fig. 5. Microscope image of grating coupler of the groove density  $\chi = 1000 \text{ g/mm}$ .

holographic master gratings. In this case, after the embossing of master grating in the sol film, the structures were calcined at 773 K (500°C) for 1.0 h. Higher calcination temperature resulted in the fact that the refractive index of waveguide films in the produced structures was higher than that in the previous case and equalled  $n_1 = 1.7818$ .

# 4. Measurement setup

The measurement setup is presented in Fig. 6. The investigated structures (PS) were placed on a goniometer (GO), which was powered by a stepping motor (SM). The rotation of the goniometer was measured with the accuracy of  $5\times10^{-4}$  degree. The grating coupler was illuminated from the substrate side. As light source, a laser diode LD of the wavelength  $\lambda=676.7$  nm powered by the generator G was applied. A respective polarization state of the illuminating beam was set using a polarizer (P) and rotator (PR). The optical signal from the edge of the structure was guided off to the detector D using a multimode fiber waveguide type PCS (200/300 µm). The detection of the modulated signal was realized with the application of a homodyne nanovoltmeter (NH). Modal spectra were recorded in the computer using a measurement card.

The incoupling angles  $\theta_r$  are determined with respect to the normal to the sensor structure surface. But the direction of the normal determined on the basis of the beam being reflected from the structure back to the laser diode is burdened with high uncertainty. Even if the beam path is lengthened to several meters, the uncertainty involving the determination of the direction of the normal is of the order of 0.05 degree. In practice, in order to reduce the determination uncertainty of the normal, we can apply the symmetry of the structure, which is excited in the diffraction orders  $r = \pm 1$  and the signals are detected from both edges of the structure (Fig. 6). In this way we obtain spectra symmetric with respect to the angle corresponding to the position of the normal. This type of detection scheme has been imple-

G D NH

Fig. 6. Measurement setup, PS – planar structure, GO – goniometer, SM – stepping motor, LD – laser diode, P – polarizer, PR – polarizer rotator, G – generator, D – detector, NH – homodyne nanovoltmeter.

mented in a commercially available computer controlled instrument Artificial Sensing Instruments (ASI): BIOS-1) [16–18]. Such a procedure can be also applied in the case of grating couplers of the lower groove density  $\chi$ , in the excitation both in the first diffraction order and in the second diffraction order. For the structures of lower groove density, a different procedure can be applied, in which the excitation in two different diffraction orders is used. Such a procedure is described below.

#### 5. Measurement results

For both types of the investigated planar structures with grating couplers, modal spectra for different refractive indexes of the cover  $n_c$  were recorded. The structures were coated with liquids whose refractive indexes were determined with the Abbe refractometer ( $\lambda_D = 589.6$  nm). The following liquids were applied, water, water solutions of glycerin and cedar oil. The obtained results are presented below.

# 5.1. Grating $\chi = 2400 \text{ g/mm}$

The structures with grating couplers of the groove density  $\chi=2400$  g/mm can be excited only in the first diffraction order, and the incoupling angles, as it follows from Eq. (1), are negative (Fig. 2). Modal spectra recorded when respectively air and water were applied as covers are presented in Fig. 7. Negative values of the incoupling angle  $\theta$  correspond to the signals recorded from the left-hand edge of the structure, and the positive values correspond to the signals recorded from the right-hand edge of the structure. We can observe sharp incoupling peaks which change their position with the change of refractive index of the cover  $n_c$ . The rise of refractive index of the cover results in the rise of the effective refractive indexes N, and, in consequence, in the rise of the value of the incoupling angles  $\theta$  (Eq. 1).

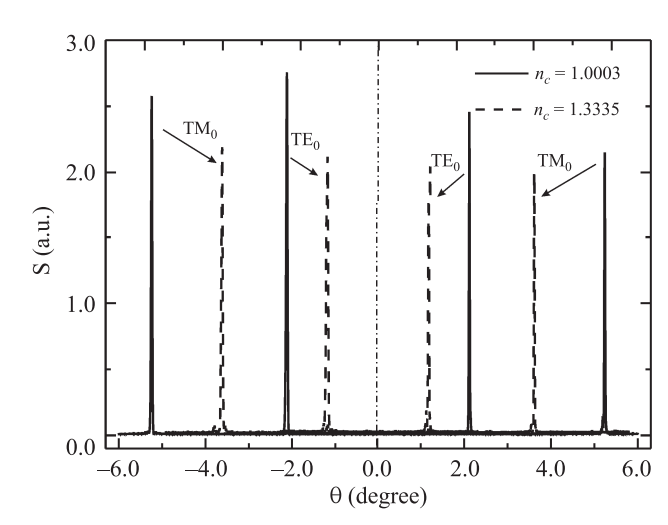


Fig. 7. Modal spectra of a planar waveguide excited with the use of grating coupler,  $\eta = 2400$  g/mm,  $\lambda = 676.7$  nm, d = 204 nm.

# 5.2. Grating $\chi = 1000$ g/mm

The waveguide structures with grating couplers of the groove density  $\chi=1000$  g/mm, in positive angle range  $\theta$  can be excited in two diffraction orders. The incoupling characteristics of TM $_0$  mode, which were recorded for the different refractive indexes  $n_c$  of the liquid covering the structure are presented in Fig. 8. Figure 8(a) presents the incoupling characteristics for the second diffraction order (r=2), and Fig. 8(b) presents the characteristics corresponding to the first diffraction order (r=1). Next to the incoupling peaks, the corresponding to them values  $n_c$  of refractive indexes of the cover were provided. It can be observed that with the rise of refractive index of the cover  $n_c$ , the incoupling angles  $\theta$  are rising.

## 6. Data evaluation and discussion

From the recorded modal spectra, for different refractive indexes of the cover  $n_c$ , corresponding to them incoupling angles were determined. The incoupling angles can be de-

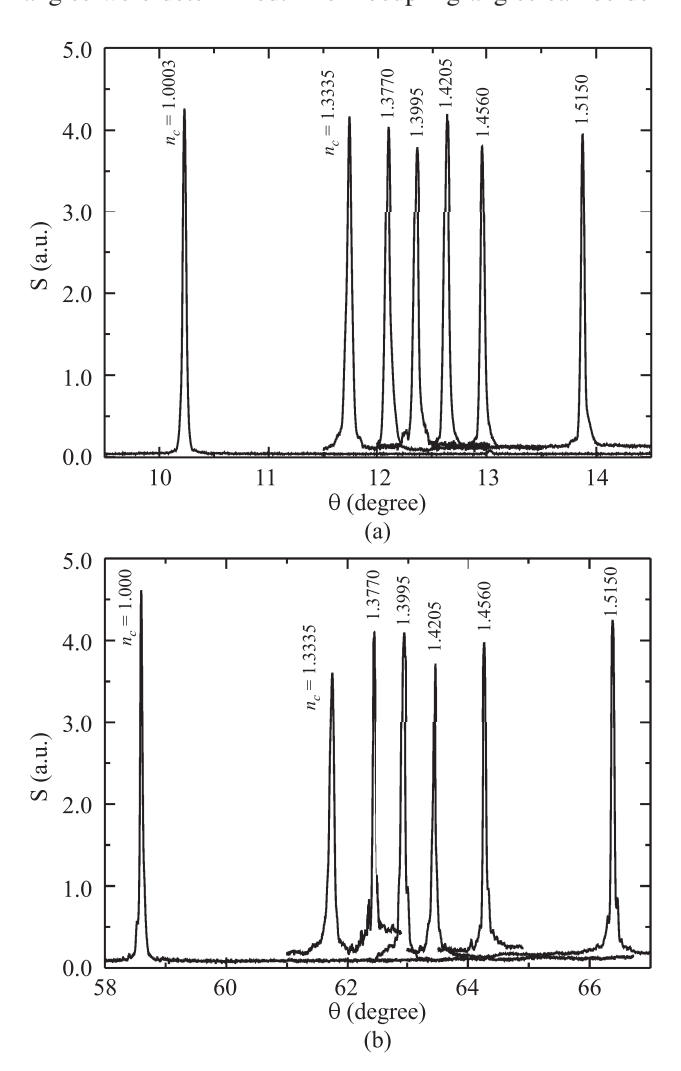


Fig. 8. Incoupling characteristics of a planar sensor structure for selected refractive indexes of a cover, (a) m = 2 and (b) m = 1, TM polarization,  $\chi = 1000$  g/mm,  $\lambda = 676.7$  nm, d = 211 nm.

termined from the maximum position of the recorded signal. However, in such a case, the determination accuracy of the incoupling angle is equal to the rotation angle of the goniometer, which corresponds to one step of the stepping motor (here 5×10<sup>-4</sup> degree). Much more accurate values of incoupling angles can be determined from the approximation of incoupling peaks by a theoretical dependence. The shape of the incoupling peak depends on the actual grating length  $L_a$ , the radius  $w_0$  of the light beam illuminating the coupler, and on the intrinsic coupling length  $L_c$ . In Ref. 23, it was demonstrated that in the case of  $w_0 \ll L_c$  and  $w_0 \ll L_g$ , the dependence of the incoupling efficiency on the angular detuning is Gaussian. In other cases, it can be Lorantz function or sinc squared function. The parameters of the presented grating couplers and the beam applied in the measurements show that the incoupling peaks should be Gaussian. It was confirmed by experimental results.

Using the approximation of incoupling peaks with Gauss function, the angle of maximum incoupling  $\theta$  was determined as well as its uncertainty  $\delta\theta$ . The points around the maximum were used for the calculations, with the signal value from  $S_{min}$  to  $S_{max}$ , where  $S_{max}$  is the maximum value of the signal in the investigated incoupling peak. By changing the value  $S_{min}$  within the range from  $0.1S_{max}$  to  $0.9S_{max}$ , the incoupling angle  $\theta$  was determined as well as its uncertainty  $\delta\theta$ . The accepted incoupling angle was the one which had the lowest uncertainty  $\delta\theta$ . Incoupling peaks of the mode  $TM_0$  (Fig. 7) recorded in the air ( $n_c = 1.0003$ ) are presented in Fig. 9. Open squares were used to mark measurement points and solid lines were used to draw up Gauss fit. In this case, the incoupling signal was recorded after two steps of the stepping motor ( $10^{-3}$  degree). For the incoupling peak presented in Fig. 9(b), the Gauss fit to the experimental run is almost ideal. For the incoupling peak presented in Fig. 9(a), for lower values of the signal S, we can observe lower Gauss fit to the experimental points. In this signal range, the peak shape is disturbed. The disturbance of incoupling peak shape can be affected by such factors as nonhomogeneity of the amplitude of coupler's corrugation, coupler's faults or non-axial position of the structure in the goniometric setup. The full widths at half maximum (FWHM) of the incoupling peaks are respectively 0.031 degree [Fig. 9(a)] and 0.023 degree [Fig. 9(b)]. The widths of the incoupling peaks determined basing on Ref. 23 (Eq. (12) are slightly smaller than the measured ones and equal 0.015 degree. The determined uncertainties of the incoupling angle are respectively  $7.0 \times 10^{-5}$  degree [Fig. 9(a)] and  $2.4 \times 10^{-5}$  degree [Fig. 9(b)]. Hence, the determination uncertainty of the incoupling angle is  $3.7 \times 10^{-5}$  degree. Therefore we can observe that using the Gauss function for the approximation of the incoupling peak we can obtain determination accuracy of the incoupling angle better than  $4\times10^{-5}$  degree. In our further discussion, the value of  $\Delta\theta_{min} = 4 \times 10^{-5}$  degree will be accepted as angular detection limit of the measurement setup.

In all cases presented here, the incoupling angles were determined by the approximation of the incoupling peaks

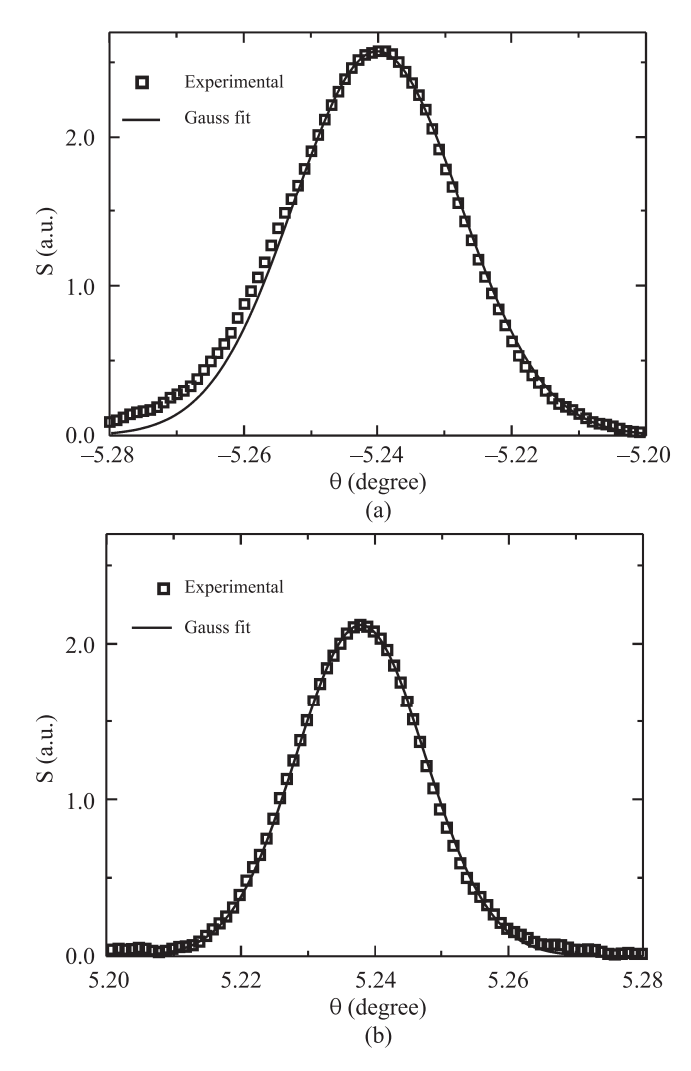


Fig. 9. Incoupling signals vs. detuning angle,  $\chi=2400$  g/mm,  $n_c=1.0003$ , (a) FWHM = 0.031 degree and (b) FWHM = 0.023

with Gauss function. Refractive indexes and the thickness of waveguide films were determined from modal equations inserting to them the measured effected indexes ( $N_{TE}$ ,  $N_{TM}$ ), when air served as the cover ( $n_c = 1.0003$ ). The results are presented in Table 1. The said parameters were applied to calculate the dependence of effective indexes on refractive indexes of the cover  $N = N(n_c)$ , which inserted to Eq. (1) yielded the dependences of incoupling angles on refractive index of the cover  $\theta(n_c)$ .

Table 1. Parameters of waveguide structures  $n_c = 1.0003$  and  $\lambda = 676.7$  nm.

|          | $\chi = 1000 \text{ g/mm}$ | $\chi = 2400 \text{ g/mm}$ |
|----------|----------------------------|----------------------------|
| $N_{TE}$ | 1.57762                    | 1.58707                    |
| $N_{TM}$ | 1.52983                    | 1.53274                    |
| d        | 211.1 nm                   | 204.2 nm                   |
| $n_1$    | 1.7609                     | 1.7818                     |

## 6.1. Grating $\chi = 2400 \text{ g/mm}$

The dependences of incoupling angles on the refractive index of the cover for the structure with a grating coupler of the groove density of  $\chi=2400$  g/mm, respectively for modes  $TE_0$  and  $TM_0$  are presented in Fig. 10. Figure 11 presents the dependences of effective indexes on the refractive index of the cover  $n_c$ . Crosses on both pictures were used to mark experimental points and solid lines to draw up theoretical dependences.

A visible rise of the curve's slope  $(\partial N/\partial n_c)$  taking place with the rise of  $n_c$  is affected by the increase in penetration depth of the evanescent field into the cover. Consequently, a part of the power of the guided mode is rising which is propagating in the cover, and the mode is becoming more sensitive to the changes of the refractive index  $n_c$  and the homogeneous sensitivity  $(\partial N/\partial n_c)$  is rising. When  $n_c > n_b$ , then the power propagating in the waveguide's cover is higher than the power propagating in the substrate [31]. Such waveguides are referred to as reverse-symmetry waveguides [32].

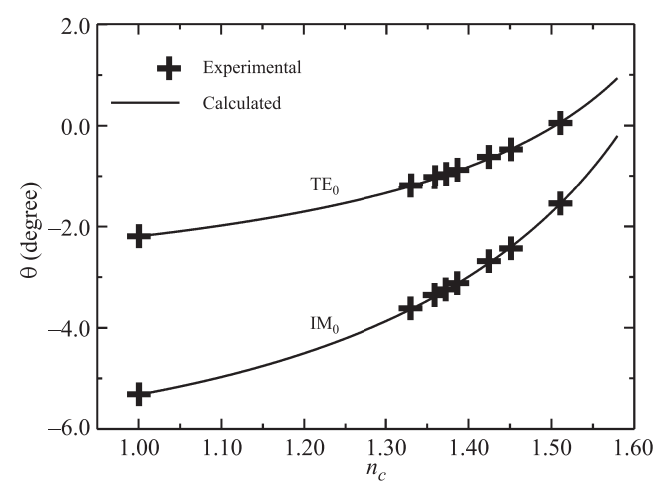


Fig. 10. Dependences of incoupling angles on refractive index of a cover,  $\chi = 2400 \text{ g/mm}$ ,  $\lambda = 676.7 \text{ nm}$ ,  $n_1 = 1.7818$ , d = 204 nm.

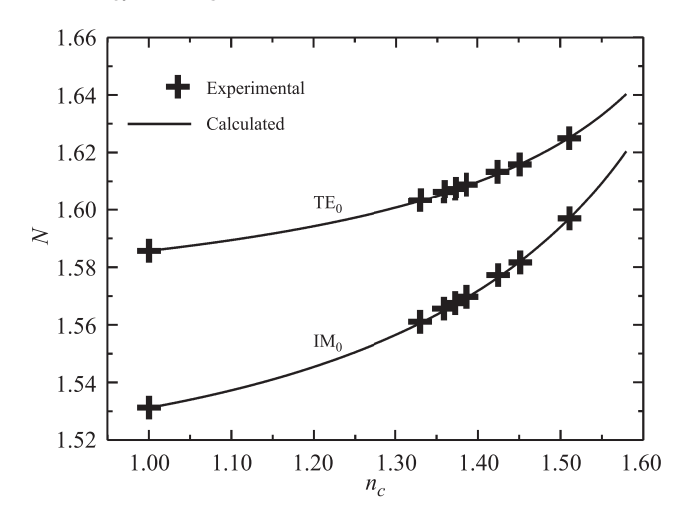


Fig. 11. Dependences of effective indexes on refractive index of a cover,  $\chi = 2400$  g/mm,  $\lambda = 676.7$  nm,  $n_1 = 1.7818$ , d = 204 nm.

# 6.2. Grating $\chi = 1000 \text{ g/mm}$

In the case when incoupling angles are at the level of single angle degrees, it is convenient to use the excitation of the structure in positive and negative diffraction order. The same measurement procedure can be applied for couplers having the lower groove density  $\chi$ , also in the cases when the excitation is taking place at higher angles. However, such a procedure considerably prolongs the measurement time. For such structures we can also apply a different procedure in which the structure is excited in the first and second diffraction order, and the signal is detected only from one edge of the structure. The following steps are to be followed in such a procedure. Initially, before the measurement, the structure is positioned approximately perpendicular to the direction of light beam incidence. Then, with a continuous change of illumination angle of the structure, the signal is recorded. From the recorded modal spectra, the approximate incoupling angles  $\theta_1$  and  $\theta_2$  are determined, i.e., the angles with respect to the initial position. When in the output position, the illumination direction of the structure differs from the true direction of the normal by  $(-\Delta\theta)$ , then also the determined angles  $\hat{\theta}_1$  and  $\hat{\theta}_2$  differ from the true values by  $(-\Delta\theta)$ . And the difference of these angles is equal to the difference of true angles. It means that basing on Eq. (1), the following system of equations can be written for each polarization

$$\sin(\tilde{\theta}_r - \Delta \tilde{\theta}) = \frac{1}{n_p} \left( N - r \frac{\lambda}{\Lambda} \right), \tag{4}$$

where r = 1, 2 is the diffraction order. After the transformations we obtain

$$\Delta \tilde{\theta} = \frac{\tilde{\theta}_1 - \tilde{\theta}_2}{2} - \arccos \left\{ \lambda \left[ 2n_p \Lambda \sin \left( \frac{\tilde{\theta}_1 - \tilde{\theta}_2}{2} \right) \right]^{-1} \right\}. (5)$$

The quantity  $\Delta \widetilde{\theta}$  determined in this way allows us to correct the recorded modal spectra to the form in which the positions of incoupling peaks correspond to true incoupling angles  $\theta_1$  and  $\theta_2$ . In Fig. 8, the corrections  $\Delta \widetilde{\theta}$  were allowed for in all characteristics.

Figure 12 presents the dependence of the incoupling angles  $\theta$  on the refractive index of the cover  $n_c$  for the first (r=1) and the second diffraction order (r=2), for the TM<sub>0</sub> mode. Crosses were used to mark the incoupling angles corresponding to the excitation of the structure in the first [Fig. 8(b)] and the second diffraction order [Fig. 8(a)], respectively. It can be observed from the comparison of dependences  $\theta(n_c)$  for both diffraction orders (Fig. 12) that the dependence of the incoupling angle on the refractive index of the cover is stronger when the structure is excited in the first diffraction order (r=1). Figure 13 presents the dependence of the effective index N on the refractive index of the cover for the TM<sub>0</sub> mode. Crosses were used to mark effective indexes, which were calculated from Eq. (1), by inserting

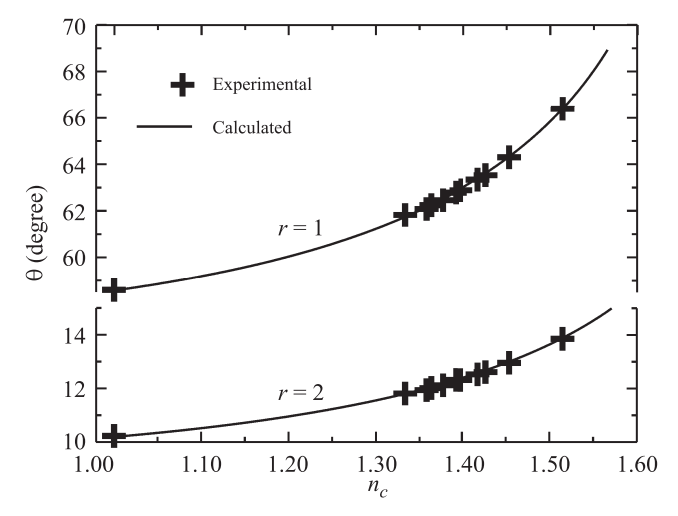


Fig. 12. Incoupling angles vs. refractive index of a cover corresponding to the first (r=1) and the second (r=2) diffraction order,  $\chi = 1000$  g/mm, TM polarization,  $\chi = 1000$  g/mm,  $\lambda = 676.7$  nm,  $n_1 = 1.7609$ , d = 211 nm.

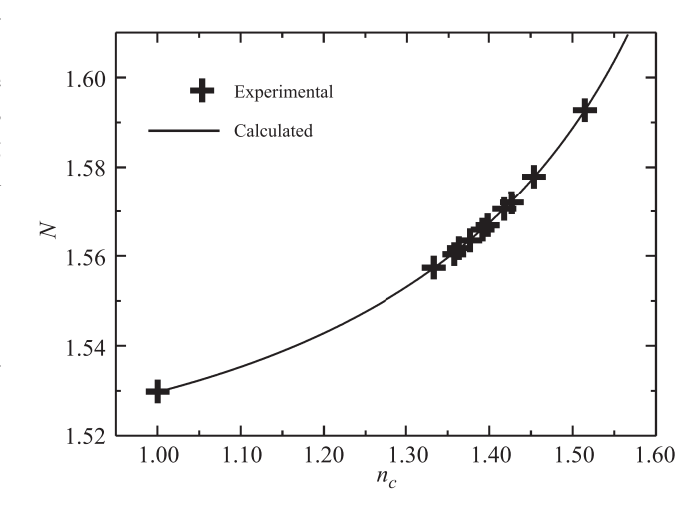


Fig. 13. Dependence of effective index on refractive index of a cover, TM polarization,  $\chi = 1000$  g/mm,  $\lambda = 676.7$  nm,  $n_1 = 1.7609$ , d = 211 nm.

the values of angles from Fig. 12 to the relation. The solid line stands for the relation calculated theoretically. We can observe an excellent agreement between the experimental points and theoretical dependence.

## 6.3. Sensitivities

Sensitivity is a parameter characterizing a sensor structure. The angle sensitivity  $(\partial\theta/\partial n_c)$  depends on optical and geometrical parameters of the waveguide film and on the grating period  $\Lambda$  (Eq. 2). The dependence of the angle sensitivities  $(\partial\theta/\partial n_c)$  on the refractive index of the cover  $n_c$  for both presented here sensor structures is presented in Fig. 14. They were obtained by differentiating the theoretical dependences from Figs. 10 and 12, respectively. It can be observed from the comparison of both figures that the lowest angle sensitivity  $(\partial\theta/\partial n_c)$  corresponds to the structure

Table 2. Sensitivities and detection limits for two different values of cover refractive indexes. TM polarization.

|                             | $n_{c}$ | $\chi = 1000 \text{ g/mm}$ $r = 1$ | $\chi = 1000 \text{ g/mm}$ $r = 2$ | $\chi = 2400 \text{ g/mm}$ $r = 1$ |
|-----------------------------|---------|------------------------------------|------------------------------------|------------------------------------|
| $\theta/\partial n_c$       | 1.33    | 16.04                              | 7.79                               | 8.19                               |
| (degree·RIU <sup>-1</sup> ) | 1.50    | 36.78                              | 15.58                              | 15.53                              |
| $(\Delta N)_{min}$ (RIU)    | 1.33    | 3.3×10 <sup>-7</sup>               | 6.8×10 <sup>-7</sup>               | 7.0×10 <sup>-7</sup>               |
|                             | 1.50    | $3.0 \times 10^{-7}$               | $6.7 \times 10^{-7}$               | $7.0 \times 10^{-7}$               |
| $(\Delta n_c)_{min}$ (RIU)  | 1.33    | 2.3×10 <sup>-6</sup>               | 5.4×10 <sup>-6</sup>               | 5.0×10 <sup>-6</sup>               |
|                             | 1.50    | $1.0 \times 10^{-6}$               | $2.6 \times 10^{-6}$               | $2.6 \times 10^{-6}$               |

with the grating coupler of the groove density of  $\chi = 2400$  g/mm, excited in the first diffraction order, with TE polarization. The highest angle sensitivity along the whole range of refractive index of the cover  $n_c$  corresponds to the structure with the grating coupler of a groove density of  $\chi = 1000$  g/mm, excited in the first diffraction order (r = 1), with TM polarization. Within the range  $n_c < 1.40$ , it is twofold higher than for r = 2. When  $n_c > 1.40$ , then the difference of angle

60  $\partial\theta/\partial n_c$  (degree RIU<sup>-1</sup>) 40 r = 11.40 1.30 1.35 1.45 1.50 1.55 1.60 (a)  $\theta\theta/\partial n_c$  (degree RIU<sup>-1</sup>)  $TM_0$ r = 21.35 1.40 1.30 1.45 1.50 1.55 1.60 (b)

Fig. 14. Influence of the refractive index of the cover on the angular sensitivities, (a)  $\chi = 2400$  g/mm and (b)  $\chi = 1000$  g/mm.

sensitivities is still higher. The values of angle sensitivities for the refractive indexes  $n_c = 1.33$  and  $n_c = 1.50$  are presented in Table 2.

#### **6.4.** Detection limits

Detection limit is a parameter characterizing the measurement system and depends on the sensitivity of sensor structure and on angular detection limit of the goniometric system. Here, the detection limit may refer to the measurement of the effective refractive index N and to the measurement of the refractive index of the cover  $n_c$ . In both cases, it means the lowest changes of the measurand  $[\Delta N_{min}]$ ,  $(\Delta n_c)_{min}$ ], which can be recorded in the measurement system. The detection limit of the measurement involving the changes of effective refractive indexes is obtained from the relation  $\Delta N_{min} = (\partial \theta / \partial N)^{-1} \Delta \theta_{min} = n_p \cos \theta_r \Delta \theta_{min}$ , where the incoupling angles  $\theta_r$  for the particular structures are taken out from the characteristics presented respectively in Figs. 10 and 12. The detection limit  $\Delta N_{min}$ , through the sensitivity  $(\partial \theta / \partial N)$ , depends on the parameters of sensor structure (Eq. 3) and on the angular detection limit of the goniometric system  $\Delta\theta_{min}$ . When the incoupling angles  $\theta_r$  are determined from the incoupling peaks symmetrical to the normal, then the angular detection limit of the measurement system is  $\Delta\theta_{min} = 4 \times 10^{-5}$  degree. And when the incoupling angles  $\theta_r$ for the coupler of the groove density  $\chi = 1000$  g/mm are determined from the peaks corresponding to different diffraction orders (r = 1, r = 2), then the location uncertainty of the incoupling peak maximum is considerably higher. The uncertainty is generated then by the grating period  $\Lambda$ , the wavelength  $\lambda$ , the refractive index of the air  $n_p$ , and the angles  $\theta$ . The grating period  $\Lambda$  can be determined with the accuracy of  $\Delta \Lambda = 0.01$  nm. The wavelength of the temperature-stabilized light source can be controlled with the accuracy of  $\Delta \lambda = 0.001$  nm. The refractive index of the air  $n_n$  can be determined from the empirical Edlen's equation [33,34]. By controlling the temperature, pressure and humidity, the refractive index of the air can be defined with the accuracy better than  $\Delta n_p = 2 \times 10^{-7}$  [34]. The uncertainty for each of the angles  $\tilde{\theta}$  is  $\Delta \tilde{\theta} = 4 \times 10^{-5}$  degree. Taking into consideration Eq. (3), the uncertainty of the incoupling angle, determined on the basis of peaks corresponding to the diffraction orders r=1 and r=2, is  $\Delta\theta_r=8\times10^{-4}$  degree. It can be now observed that in this case, the angle detection limit of the system is 20 times worse than in the case where the peaks symmetrical to the normal have been applied.

The measurement detection limit involving the changes of refractive index of the cover is obtained from the dependence  $(\Delta n_c)_{min} = (\partial \theta' \partial n_c)^{-1} \Delta \theta_{min}$ , where the angle sensitivities  $(\partial \theta' \partial n_c)$  are taken from the characteristics presented in Fig.14. For the polarization TM, there are the higher angle sensitivities, and hence lower detection limits involving the changes of refractive index of the cover  $(\Delta n_c)_{min}$  than for the polarization TE. The calculated limits of detection involving the changes of the effective refractive index  $(\Delta N)_{min}$  and the refractive index of the cover  $(\Delta n_c)_{min}$  for the presented sensor structures, when the incoupling angles are determined basing on peaks symmetrical to the normal ( $\Delta \theta_{min}$  = 4×10<sup>-5</sup> degree) are presented in Table 2. The results correspond to the polarization TM and refractive indexes of the cover  $n_c = 1.33$  and  $n_c = 1.50$ , respectively. For the structure of groove density of  $\chi = 1000$  g/mm, when the incoupling angles are determined basing on the incoupling peaks corresponding to different diffraction orders (r = 1, r = 2), the detection limits  $(\Delta N)_{min}$  and  $(\Delta n_c)_{min}$  are 20-fold higher.

#### 6.5. Discussion

Table 2 presents angle sensitivities and detection limits for the true sensor structures presented in the paper when the incoupling angles are determined on the basis of the peaks symmetrical to the normal ( $\Delta\theta_{min} = 4 \times 10^{-5}$  degree). Both, the angular sensitivity and detection limits for the structure of the groove density of  $\chi = 2400$  g/mm (r = 1) are almost identical, as for the structure of the groove density of  $\chi =$ 1000 g/mm excited in the second diffraction order (r = 2). And the angle sensitivity of the structure of the groove density of  $\chi = 1000$  g/mm, excited in the first diffraction order (r = 1) is about two-fold higher than the angle sensitivity of the structure of the groove density of  $\chi = 2400$  g/mm. At the same time, the detection limits respectively of the effective refractive index  $(\Delta N)_{min}$  and of the refractive index of the cover  $(\Delta n_c)_{min}$  are over two-fold lower. It is affected by the influence of the grating period  $\Lambda$  on the sensitivity  $(\partial \theta / \partial N)$ (Fig. 3). We can observe, however, that in the absolute scale these differences are inconsiderable, and in practice they are not likely to determine the choice of the groove density  $\chi$  of the coupler. In many practical applications, a shorter measurement time is much more important. Therefore, the structures with grating couplers of the high groove density  $\gamma$  are frequently preferred. The obtained detection limits involving the change of effective refractive index  $(\Delta N)_{min}$  and the refractive index of the cover  $(\Delta n_c)_{min}$  are comparable with the parameters of the commercially available instrument [18], as well as with the parameters of similar structures presented by other authors [1,35–38]. In Ref. 38, an overview

on different types of grating coupler sensors and their detection limits is presented.

In practice, the sensor structures are optimized into higher measurement ranges to obtain higher sensitivities and lower detection limits. The angle sensitivity  $(\partial\theta'\,\partial n_c) = (\partial\theta'\,\partial N)\cdot(\partial N'\,\partial n_c)$  can be shaped within a certain range through the sensitivity  $(\partial\theta'\,\partial N)$  (Fig. 3) and through the homogeneous sensitivity  $(\partial N'\,\partial n_c)$ . The homogeneous sensitivity is rising with the rise of the contrast between the refractive indexes of the waveguide film and the cover [1,31]. The simplest way to obtain the increase in contrast of refractive indexes in the presented structures is the application of substrates of lower refractive index. The application of silica glass substrates will additionally allow us to apply higher calcination temperatures which can, in turn, yield more compact waveguide films of still higher refractive index, which can also contribute to the rise of sensitivity.

Figure 15 presents theoretical dependences of detection limits involving the changes of refractive index of the cover  $(\Delta n_c)_{min}$  on the thickness d of the waveguide film for two

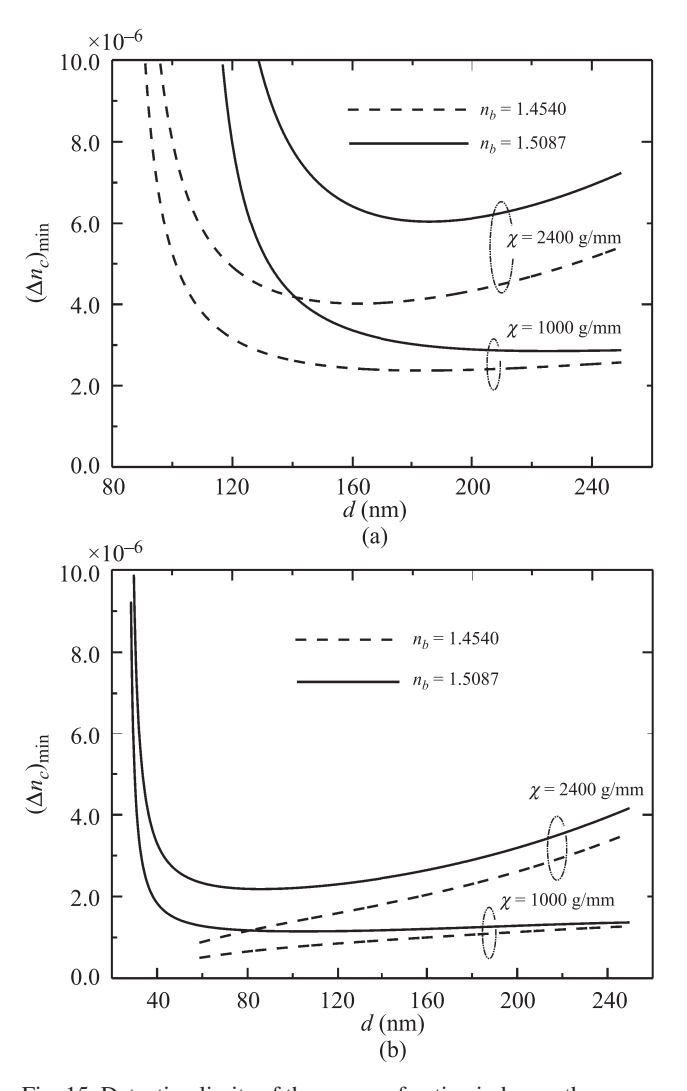


Fig. 15. Detection limits of the cover refractive index on the waveguide film thickness for different substrate refractive indexes,  $n_1 = 1.7818$ ,  $\lambda = 676.7$  nm, (a)  $n_c = 1.33$  and (b)  $n_c = 1.50$ .

Table 3. Detection limits for optimal film thickness and different substrate refractive indexes  $n_1 = 1.7818$  and  $\lambda = 676.7$  nm.

| $n_c$ | $n_b$  | $\chi = 1000 \text{ g/mm}$ $r = 1$ |                            | $\chi = 2400 \text{ g/mm}$ $r = 1$ |                            |
|-------|--------|------------------------------------|----------------------------|------------------------------------|----------------------------|
|       |        | $d_{opt}$ (nm)                     | $(\Delta n_c)_{min}$ (RIU) | $d_{opt}$ (nm)                     | $(\Delta n_c)_{min}$ (RIU) |
| 1.33  | 1.5087 | 225.3 nm                           | 2,8×10 <sup>-6</sup>       | 185.5 nm                           | 6.0×10 <sup>-6</sup>       |
|       | 1.4540 | 183.2 nm                           | $2.4 \times 10^{-6}$       | 162.3 nm                           | 4.0×10 <sup>-6</sup>       |
| 1.50  | 1.5087 | 104.5 nm                           | $1.1 \times 10^{-6}$       | 86.0 nm                            | 2.2×10 <sup>-6</sup>       |
|       | 1.4540 | 58.5 nm                            | $0.5 \times 10^{-6}$       | 58.5 nm                            | $0.9 \times 10^{-6}$       |

different refractive indexes of the substrate. The calculations were carried out for the structures of soda-lime glass substrates (solid lines)  $n_b = 1.5087$  and silica glass substrates (dashed lines)  $n_b = 1.4540$ . For the calculations we accepted the refractive index of the waveguide film of one of the presented structures  $n_1 = 1.7818$  and refractive indexes of the cover respectively  $n_c = 1.33$  [Fig.15(a)] and  $n_c = 1.50$  [Fig. 15(b)]. For both refractive indexes of the cover  $n_c$ , the structures with the substrate of lower refractive index have lower detection limits  $(\Delta n_c)_{min}$ . The characteristics corresponding to the refractive indexes  $n_b = 1.4540$  and  $n_c = 1.50$  [Fig. 15(b)] have different run from the other ones. It results from the fact that these are structures with reverse--symmetry waveguides. Sensor properties of reverse-symmetry waveguides have been investigated by Horváth et al. [32,39,40]. In such structures  $(n_c > n_b)$ , for the thickness d of the waveguide film slightly higher than the cut-off thickness, the homogeneous sensitivity is close to unit value [2,31,32], and it means that in such a case the detection limit  $(\Delta n_c)_{min}$  is limited solely by the angular detection limit of the goniometer. Table 3 presents the minimum values of detection limits  $(\Delta n_c)_{min}$  and corresponding to them thicknesses of the waveguide films  $d_{opt}$  (Fig. 15). We can observe that for  $n_c = 1.33$ , the detection limits  $(\Delta n_c)_{min}$  of the presented structures (Table 2) are slightly higher than the obtainable ones, with optimal thicknesses of waveguide films  $d_{opt}$ .

The improvement in the detection limits  $(\Delta N)_{min}$  and  $(\Delta n_c)_{min}$ , for the sensor structures involving the refractive indexes of the cover  $n_c \approx 1.33$  ( $n_c < n_b$ ), can be obtained by the application of waveguide films of higher refractive indexes than those presented in the work. The structures produced with the use of tantalum pentoxide  $\text{Ta}_2\text{O}_5$  (n=2.22) were presented in Refs. 13, 14, 38, 41, and 42. Cottier *et al.* [34] refer that for the measurement of refractive index of water solutions of glycerin they obtained the detection of  $< 10^{-6}$  RIU. The structures produced with the application of titania  $\text{TiO}_2$  (n=2.38) were presented in Refs. 15, 42, and 43. However, the application of tantalum pentoxide or titania necessitates the application of other production technologies of waveguide films and grating couplers different from those presented in the work.

The waveguide films produced with the application of sol-gel method are characterized by microporosity, which brings about the change of their refractive index when contacted with liquid [1]. Liquid particles penetrate the micropores of the waveguide film SiO<sub>2</sub>:TiO<sub>2</sub>, which leads to the fluctuation of effective refractive indexes, and in consequence to the reduction of the detection limit of effective refractive indexes to about  $(\Delta N)_{min} = (1-2) \times 10^{-6}$  RIU [44]. The said effect can be reduced by calcination the structures at higher temperatures (~850°C), but then we must apply silicon substrates with a silica film or silica glass substrates. The way to correct the drift of effective refractive indexes in the system of output grating coupler has been presented in Ref. 45. In some cases as, e.g., in gas chemical sensors, the drift affected by the change of the refractive index of waveguide film can be controlled by the application of a reference path. Such a solution is particularly grounded due to a simultaneous correction of the influence of temperature on sensor structure parameters [42]. In the measurements of the refractive index of liquids, the achievement of low detection limit of the refractive index  $(\Delta n_c)_{min}$  offered by the measurement setup requires that the temperature stabilization should be applied. The thermo-optical coefficient of water is  $(\partial n_c / \partial T)_{\text{H}_2\text{O}} = -110.6 \times 10^{-6} \text{ RIU} \cdot \text{K}^{-1}$  [42]. It means that the influence of temperature on the refractive index of water, when investigating water solutions ( $n_c \sim 1.33$ ), makes it impossible to apply high sensitivities which are offered by sensor structures based on tantalum pentoxide waveguides and titania waveguides. The resolution is limited by temperature fluctuations. In practice, it is possible to ensure temperature stabilization at the level of 0.1-0.2 K [20,44,45], which means that the detection limit involving the measurement of refractive index changes is limited to the level of  $(\Delta n_c)_{min}$  $\sim 10^{-5}$  RIU. Hence, we can observe that the sensitivities of sensor structures presented in the work are sufficient for the measurements of refractive indexes of water solutions and can be applied in biochemical measurements.

## 7. Conclusions

The paper presents research results on planar sensor structures with grating couplers of the groove densities respectively  $\chi = 1000$  g/mm and  $\chi = 2400$  g/mm. Waveguide films SiO<sub>2</sub>:TiO<sub>2</sub> were obtained using the sol-gel method, and grating couplers were produced by master grating embossing in

the sol film. The presented sensor structures are characterized by Gaussian narrow incoupling characteristics. It has been demonstrated that through fitting the incoupling of Gauss function to the characteristics, we can improve the angular detection limit of the goniometric system. It has been demonstrated that lower groove densities of the grating  $\chi$  correspond to the lower detection limits of effective indexes and refractive indexes of the cover. The estimated detection limits of the structure of the groove density  $\chi = 1000$ g/mm, excited in the  $\pm 1^{-st}$  diffraction order are respectively,  $\Delta N_{min} = 3.3 \times 10^{-7} \text{ RIU for } n_c = 1.33 \text{ and } \Delta N_{min} = 3.0 \times 10^{-7}$ RIU for  $n_c = 1.50$ . The detection limits of the refractive index of the cover are  $(\Delta n_c)_{min} = 2.3 \times 10^{-6}$  RIU, when  $n_c = 1.33$ and  $(\Delta n_c)_{min} = 1.0 \times 10^{-6}$ , when  $n_c = 1.500$ . For the structure of the groove density  $\chi = 2400$  g/mm, the limit values are over twofold higher, but their advantage is that they are characterized by small excitation angles and shorter measurement times.

For the structure of the groove density of  $\chi=1000$  g/mm, the incoupling angles can be determined from the position of peaks corresponding to the excitation of the structure in the 1<sup>st</sup> and in the 2<sup>nd</sup> diffraction order. But then, the detection limits are 20-fold higher. The influence of temperature on the refractive indexes is reducing the detection limits of refractive index changes to the level of ~10<sup>-5</sup> RIU.

The work financed by the Polish Ministry of Science and Higher Education within the Grant N 515 057 31/2432.

## References

- W. Lukosz, "Integrated optical chemical and direct biochemical sensors", Sensor. Actuator. B29, 37–50 (1995).
- 2. K. Tiefenthaler and W. Lukosz, "Sensitivity of grating couplers as integrated-optical chemical sensors", *J. Opt. Soc. Am.* **B6**, 209–220 (1989).
- 3. P.M. Nellen and W. Lukosz, "Integrated input grating coupler as chemo- and immunosensors", *Sensor. Actuator.* **B1**, 592–596 (1990).
- M. Błahut, R. Rogoziński, P. Karasiński, K. Gut, and A. Opilski, "Model of planar refractometer based on two-port interferometer on glass", *Opt. Appl.* 24, 171–177 (1994).
- P. Hua, B.J. Juff, G.R. Quigley, J.S. Wilkinson, and K. Kawaguchi, "Integrated optical dual Mach-Zehnder interferometer sensor", *Sensor. Actuator.* B87, 250–257 (2002).
- 6. A. Brandenburg and R. Henninger, "Integrated optical Young interferometer", *Appl. Optics* **33**, 5941–5947 (1994).
- A. Ymeti, J. Greve, P.V. Lambeck, T. Wink, S.W.F.M. Hovell, T.A.M. Beumer, R.R. Wijn, R.G. Heideman, V. Subramaniam, and J.S. Kanger, "Fast, ultrasensitive virus detection using a Young interferometer sensor", *Nano Lett.* 7, 394–397 (2007).
- C. Stamm and W. Lukosz, "Integrated optical difference interferometer as immunosensor", *Sensor. Actuator.* B31, 203–207 (1996).
- 9. C. Stamm, R. Dangel, and W. Lukosz, "Biosensing with the integrated-optical difference interferometer: dual-wavelength operation", *Opt. Commun.* **153**, 347–359 (1998).

- T. Koster and P.V. Lambeck, "Fully integrated optical polarimeter", Sensor, Actuator. B82, 213–226 (2002).
- K. Tiefenthaler and W. Lukosz, "Integrated optical switches and gas sensors", Opt. Lett. 10, 137–139 (1984).
- 12. K. Tiefenthaler and W. Lukosz, "Grating couplers as integrated optical humidity and gas sensors", *Thin Solid Films* **126**, 205–211 (1985).
- 13. R.E. Kunz, "Gradient effective index waveguide sensors", *Sensor. Actuator.* **B11**, 167–176 (1993).
- 14. R.E. Kunz and L.U. Kempen, "Miniature integrated optical sensors", *Proc. SPIE* **2068**, 69–85 (1994).
- M. Wiki, H. Gao, M. Juvet, and R.E. Kunz, "Compact integrated optical sensor system", *Biosens. Bioelectron.* 16, 37–45 (2001).
- J. Vörös, J.J. Ramsden, G. Csúcs, I. Szendrö, S.M. De Paul, M. Textor, and N.D. Spencer, "Optical grating coupler biosensors", *Biomaterials* 23, 3699–3710 (2003).
- R. Horváth, G. Fricsovszky, and E. Papp, "Application of the optical waveguide lightmode spectroscopy to monitor lipid bilayer phase transition", *Biosens. Bioelectron.* 18, 415–428 (2003).
- 18. http://www.microvacuum.com
- J. Homola, S.S. Yee, and G. Gauglitz, "Surface plasmon resonance sensors: review", Sensor. Actuator. B54, 3–15 (1999).
- X.D. Hao, A.G. Kirk, and M. Tabrizan, "Towards integrated and sensitive surface plasmon resonance biosensors: A review of recent progress", *Biosens. Bioelectron.* 23, 151–160 (2007).
- C.J. Brinker and G.W. Scherer, Sol-gel Science, Academic Press, Inc. San Diego, 1990.
- 22. K. Heuberger and W. Lukosz, "Embossing technique for fabricating surface relief gratings on hard oxide waveguides", *Appl. Optics* **25**, 1499–1504 (1986).
- 23. J. Brazas and L. Li, "Analysis of input-grating couplers having finite lengths", *Appl. Optics* **34**, 3786–3792 (1995).
- P. Karasiński, "Dielectric layers SiO<sub>2</sub>:TiO<sub>2</sub> produced using the sol-gel technology for the application in planar sensors", *Proc. SPIE* 5576, 176–180 (2004).
- 25. P. Karasiński, "Sol-gel derived optical waveguide films for planar sensors with phase modulation", *Opt. Appl.* **34**, 467–475 (2004).
- 26. K. Wörhoff, P.V. Lambeck, and A. Driessen, "Design, tolerance analysis, and fabrication of silicon oxynitride based planar optical waveguides for communication devices", *J. Lightwave Technol.* 17, 1401–1407 (1999).
- 27. P. Karasiński, J. Jaglarz, and J. Mazur, "Low loss silica-titania waveguide films", *Photonics Letters of Poland* 2, (2010).
- 28. W. Lukosz and K. Tiefenthaler, "Embossing technique for fabricating integrated optical components in hard inorganic waveguiding materials", *Opt. Lett.* **8**, 537–539 (1983).
- 29. I. Szendrö, "Art and practice to emboss gratings into sol-gel waveguides", *Proc. SPIE* **4284**, 80–87 (2001).
- P. Karasiński, J. Jaglarz, and J. Mazur, "Characterization of low loss silica-titania waveguide films". (in preparation)
- 31. P. Karasiński, "Sensor properties of planar waveguide structures with grating couplers", *Opto-Electron. Rev.* **15**, 168–178 (2007).
- 32. R. Horváth, L.R. Lindvold, and N.B. Larsen, "Revers-symmetry waveguides: theory and fabrication", *Appl. Phys.* **B74**, 383–393 (2002).

- 33. G. Bönsch and P. Potulski, "Measurement of the refractive index of air and comparision with modified Edlén's formulae", *Metrologia* **35**, 133–139 (1998).
- R.B.S. Neto, J.P.R.F. de Mendonça, and B. Lesche, "Determination of absolute values of refractive index of liquids using an interferometric method", *Revista de Física Aplicada e Instrumentação* 17, 74–79 (2004).
- W.A. Challener, J.D. Edwards, R.W. McGowen, J. Skorjanec, and Z. Yang, "A multiplayer grating-based evanescent wave sensing technique", Sensor. Actuator. B71, 42–46 (2000).
- K. Cottier, M. Wiki, G. Viorin, H. Gao, and R.E. Kunz, "Label-free sensitive detection of (small) molecules by wavelength interrogation of integrated optical chips", *Sensor. Actuator.* B91, 241–251 (2003).
- S. Grego, J.R. McDaniel, and B.R. Stoner, "Wavelength interrogation og grating-based optical biosensors in the coupler configuration", Sensor, Actuator. B131, 347–355 (2008).
- 38. K. Schmitt, K. Oehse, G. Sulz, and C. Hoffman, "Evanescent field sensors based on tantalum pentoxide waveguides-a review", *Sensors* 8, 711–738 (2008).
- 39. R. Horváth and H.C. Pedersen, "Demonstration of reverse symmetry waveguide sensing in aqueous solution", *Appl. Phys. Lett.* **81**, 2166–2168 (2002).

- R. Horváth, H.C. Pedersen, N. Skivesen, C. Svanberg, and N.B. Larsen, "Fabrication of reverse symmetry polymer waveguide sensor chips on nanoporous substrates using dip-floating", *J. Micromech. Microeng.* 15, 1260–1264 (2005).
- A. Brandenburg, R. Polzius, F. Bier, U. Bliltewski, and E. Wagner, "Direct observation of affinity of reactions by reflected-mode operation of integrated optical grating coupler", *Sensor. Actuator.* B30, 55–59 (1996).
- 42. J. Dübendorfer and R.E. Kunz, "Reference pads for miniature integrated optical sensors", *Sensor. Actuator.* **B38/39**, 116–121 (1997).
- M. Wiki and R.E. Kunz, "Wavelength-interrogated optical sensor for biochemical applications", *Opt. Lett.* 25, 463–465 (2000).
- D. Clarc and W. Lukosz, "Integrated optical output grating coupler as refractometer and (bio-)chemical sensor", *Sensor.* Actuator. B11, 461–465 (1993).
- D. Clarc and W. Lukosz, "Direct immunosensing with an integrated-optical output grating coupler", *Sensor. Actuator.* B40, 53–58 (1997).